Correlating Electronic Structure with Cycling Performance of Substituted LiMn₂O₄ Electrode Materials: A Study Using the Techniques of Soft X-ray Absorption and Emission

M. M. Grush,*,†,# C. R. Horne,▽,‡,§ R. C. C. Perera,§ D. L. Ederer,‖ S. P. Cramer,‡,⊥ E. J. Cairns,‡,§ and T. A. Callcott†

University of Tennessee, Knoxville, Tennessee 37996; University of California, Berkeley, California 94720; Lawrence Berkeley National Laboratory, Berkeley, California 94720; Tulane University, New Orleans, Louisiana 70118; and University of California, Davis, California 95616

Rechargeable batteries using LiMn₂O₄ cathodes are commercially attractive, if the problem of excessive capacity fading can be overcome. The cycling properties of these systems can be improved by partial metal substitution for the Mn. To understand the correlation between electrode performance and composition, Mn, Co, and Ni L-edge XAS and XES spectra of a series of LiMn₂₋ᵧMeᵧO₄ samples (Me = Co, Ni, Li) were recorded. Cobalt is shown to substitute into the spinel system as Co(III) and nickel as Ni(II). A positive correlation between the cycling stability of the electrode and the covalency of the Mn is observed.

Introduction

Rechargeable batteries based on LiMn₂O₄ cathodes have been suggested as a commercially viable alternative to the current nickel- and cobalt-based systems due to their relatively high specific energy, low toxicity, and low cost.[1] The useful cycling range of these systems is 3.0−4.4 V (vs Li/Li⁺), with the electrode cycling between LiMn₂O₄ and a delithiated form, LiₓMn₂O₄ (0.05 ≤ x ≤ 0.20).[2−4] The electrochemically delithiated LiₓMn₂O₄ is structurally similar to the chemically prepared spinel, λ-MnO₂.[4] Both LiMn₂O₄ and the delithiated LiₓMn₂O₄ possess a spinel structure (A[B₂]O₄) where the Li atoms occupy the "A" or tetrahedral sites and the Mn atoms occupy "B" or octahedral sites. The Mn⁴⁺ atoms in LiMn₂O₄ possess cubic symmetry whereas the Mn³⁺ atoms undergo a Jahn−Teller distortion[5,6] that causes an expansion of the spinel lattice. Successive expansion and contraction of the lattice during cycling of the electrode can cause structural breakdown. This is thought to be a major contributor to the capacity fading observed upon repeated cycling[7] which prevents these systems from being successfully commercialized.

Partial substitution of metal cations for the Mn can significantly improve the cycling of these electrode materials,[7−11] but at the expense of a decrease in initial capacity within the useful voltage window (i.e., below 4.5 V). It has been suggested that the lowered initial capacity in LiMn₂₋ᵧMeᵧO₄ electrodes (Me = metal) is due to the increase of Mn⁴⁺ and corresponding decrease of Mn³⁺ in the substituted systems, as compared to LiMn₂O₄.[9,12] Less Mn³⁺ should lead to less tetragonal distortion and result in a reduced probability of structural breakdown and enhanced cycling performance.[7]

Many studies have shown substitution to enhance the cycling stability of LiMn₂O₄-based electrodes; a few also contrast the effect of different metal substituents over a range of substitution levels.[9,10,13] (We note that comparing data from different groups is exceedingly difficult and can be very misleading due to the variations in cycling conditions employed.) The capacity retention after 80 cycles of both Co and Ni substituted electrodes, as found by Liu and co-workers,[10] is tabulated and plotted in the Appendix. For a given nominal

* To whom correspondence should be addressed.
† University of Tennessee.
‡ University of California, Berkeley.
§ Lawrence Berkeley National Laboratory.
‖ Tulane University.
⊥ University of California, Davis.
Present address: Stanford Synchrotron Radiation Laboratory, Stanford, CA 94309.
▽ Present address: NanoGram Corporation, Fremont, CA 94538.

(1) Tarascon, J. M.; Guyomard, D. *Electrochem. Acta* **1993**, *38*, 1221.
(2) Hunter, J. C. *J. Sol. State Chem.* **1981**, *39*, 142.
(3) Goodenough, J. B.; Thackeray, M. M.; David, W. I. F.; Bruce, P. G. *Rev. Chem. Miner.* **1984**, *21*, 435.
(4) Mosbah, A.; Verbaere, A.; Tournoux, M. *Mater. Res. Bull.* **1983**, *18*, 1375.
(5) Cairns, E. J.; Horne, C. R.; Weiss, B. J. R.; Grush, M. M.; Cramer, S. P. Proceedings of the 2nd International Symposium on new Materials for Fuel Cells and Modern Battery Systems; Savadago, O., Roberge, P. R., Eds.; Montreal, July 6−10, 1997; Ecole Polytechnique de Montreal: Montreal, 1997.
(6) Yamaguchi, H.; Yamada, A.; Uwe, H. *Phys. Rev. B* **1998**, *58*, 8.
(7) Gummow, R. J.; de Kock, A.; Thackeray, M. M. *Solid State Ionics* **1994**, *69*, 59.
(8) Bittihn, R.; Herr, R.; Hoge, D. *J. Power Sources* **1993**, *43−44*, 223.
(9) Guohua, L.; Ikuta, H.; Uchida, T.; Wakihara, M. *J. Electrochem. Soc.* **1996**, *143*, 178.
(10) Liu, W.; Kowal, K.; Farrington, G. C. *J. Electrochem. Soc.* **1996**, *143*, 3590.
(11) Amine, K.; Tukamoto, H.; Yasuda, H.; Fujita, Y. *J. Electrochem. Soc.* **1996**, *143*, 1607.
(12) Yoshio, M. *Prog. Batteries Battery Mater.* **1997**, *16*, 252.
(13) Pistoia, G.; Antonini, A.; Rosati, R.; Bellitto, C.; Ingo, G. M. *Chem. Mater.* **1997**, *9*, 1443.

oxidation state of Mn, data from Liu et al. indicate that electrodes that have been substituted with Co cycle more stably than those that have been substituted with Ni. However, the relationship between the type and amount of metal substitution and the cycling enhancement has not been adequately explained. It has been suggested that the metal−oxygen bond strength may play a role in the integrity of the spinel and thus the electrode behavior although a clear correlation between bond strength and cycling stability was not observed.[9] In addition, a change in covalency resulting from different metal substituents may affect the cycling properties in partially substituted electrodes.[14]

Much effort has been devoted to using X-ray absorption spectroscopy (XAS) to study transition metal catalytic systems, taking advantage of the element-specific nature of this technique. Both "soft" (100−1200 eV) and "hard" (1200−12000 eV) XAS have been used to investigate a variety of metal centers, although predominantly "hard" XAS, namely XANES and EXAFS, has been applied to date in the study of $LiMn_2O_4$ batteries.[5,6,15−20] The benefit of using "soft" X-rays to study 3d transition metals is the longer core hole lifetime of the L-edge transitions which occur in this region, compared to the corresponding K-edges in the "hard" X-ray regime. This decrease in line width leads to better-resolved features in the spectra. $L_{II,III}$-edge XAS of transition metals can be a sensitive probe of the oxidation and spin state of transition metal sites, as has been shown previously.[21−26]

In addition, L-edge X-ray emission spectroscopy (XES) of transition metals is a highly sensitive probe of covalency. Changes in the L-emission spectra as a function of oxidation for first row transition metals were first reported by Fischer using electron excitation.[27] The dependence of the L-XES on both the oxidation state and the covalency of Cu compounds has been intensely investigated.[28−31] The higher the degree of covalency,

the larger the ratio of L_α/L_β. This effect has also been observed for Mn complexes using Bremsstrahlung from a chromium X-ray tube for the excitation radiation.[32] We have more recently probed similar systems using monochromatic synchrotron radiation and have obtained spectra with better statistics and resolution.[33]

To probe the covalency and to better understand the correlation between electrode performance and electrode composition, we have measured soft X-ray absorption and emission spectra on a series of $LiMn_{2−y}Me_yO_4$ electrode materials (Me = Co, Ni, Li and $0 \leq y \leq 0.5$). This work constitutes, to our knowledge, the first combined soft X-ray absorption and emission study of $LiMn_2O_4$-based electrode materials.

Experimental Section

Manganese L-absorption experiments were performed on Beamline 6.3.2 at the Advanced Light Source (located at Lawrence Berkeley National Laboratory). This is a bend magnet beamline with a Hettrick−Underwood-type monochromator capable of high-energy resolution.[34] A 1200 lines/mm grating with an exit slit of 13.5 μm resulted in a resolving power ($E/\Delta E$) of better than 4800 at the Mn L_{III}-edge. The monochromator position was calibrated as has been previously described.[34] The manganese absorption was recorded by using a Galileo channeltron to monitor the electron yield from the sample as a function of excitation energy. The incident intensity (I_m) of the X-ray beam was recorded as the current from the refocusing mirror. To take into account any differences between I_m and the incident intensity on the sample, a spectrum was recorded which consisted of the incident beam intensity measured with a pop-in photodiode just upstream of the sample divided by the mirror current (I_0/I_m). The absorption spectra were divided by the I_m recorded simultaneously with the absorption from the sample and then by (I_0/I_m). A linear background fit to the preedge region was subtracted from the spectra which were then normalized to unit intensity at the L_{II}-peak.

Cobalt and nickel L-absorption spectra were measured on Beamline 8.0.1 at the Advanced Light Source. This is an undulator beamline with a spherical grating monochromator, as has been previously described.[35] A 925 lines/mm grating with entrance and exit slits of 25 μm resulted in a resolving power of ∼4000. The transition metal L-absorption spectra were measured by collecting the total sample current and dividing by the incident intensity monitored by the current from a gold mesh in the beampath. The background and normalization procedure was the same as that described for the Mn data. Spectra were energy calibrated by comparison to data recorded previously on Beamline 6.3.2.

Manganese, cobalt, and nickel emission measurements were recorded using the University of Tennessee soft X-ray fluorescence endstation located on Beamline 8.0.1 at the Advanced Light Source. A 925 lines/mm grating was used to monochromatize the above threshold excitation energy for the emission

(14) Gee, B.; Horne, C. R.; Cairns, E. J.; Reimer, J. A. *J. Phys. Chem. B* **1998**, *102*, 10142.

(15) Horne, C. R.; Weiss, B. J. R.; Bergmann, U.; Grush, M. M.; Cairns, E. J.; Cramer, S. P. Manuscript submitted to *Phys. Rev. B*, 1999.

(16) Liu, R. S.; Jang, L. Y.; Chen, J. M.; Tsai, Y. C.; Hwang, Y. D.; Liu, R. G. *J. Solid State Chem.* **1997**, *128*, 326.

(17) Ammundsen, B.; Jones, D. J.; Rozière, J. *J. Solid State Chem.* **1998**, *141*, 294.

(18) Shinshu, F.; Kaida, S.; Nagayama, M.; Nitta, Y. *J. Power Sources* **1997**, *68*, 609.

(19) Shiraishi, Y.; Nakai, I.; Tsubata, T.; Himeda, T.; Nishikawa, F. *J. Solid State Chem.* **1997**, *133*, 587.

(20) Treuil, N.; Labrugère, C.; Menetrier, M.; Portier, J.; Campet, G.; Deshayes, A.; Frison, J.-C.; Hwang, S.-J.; Song, S.-W.; Choy, J.-H. *J. Phys. Chem. B* **1999**, *103*, 2100.

(21) Cramer, S. P.; de Groot, F. M. F.; Ma, Y.; Chen, C. T.; Sette, F.; Kipke, C. A.; Eichhorn, D. M.; Chan, M. K.; Armstrong, W. H.; Libby, E.; Christou, G.; Brooker, S.; McKee, V.; Mullins, O. C.; Fuggle, J. C. *J. Am. Chem. Soc.* **1991**, *113*, 7937.

(22) Grush, M. M.; Chen, J.; Stemmler, T. L.; George, S. J.; Ralston, C. Y.; Stibrany, R. T.; Gelasco, A.; Christou, G.; Gorun, S. M.; Penner-Hahn, J. E.; Cramer, S. P. *J. Am. Chem. Soc.* **1996**, *118*, 65.

(23) de Groot, F. M. F.; Abbate, M.; Van Elp, J.; Sawatzky, G. A.; Ma, Y. J.; Chen, C. T.; Sette, F. *J. Phys. Condens. Matter* **1993**, *5*, 2277.

(24) de Groot, F. M. F.; Fuggle, J. C.; Thole, B. T.; Sawatzky, G. A. *Phys. Rev. B* **1990**, *42*, 5459.

(25) Suzuki, S.; Tomita, M.; Okada, S.; Arai, H. *J. Phys. Chem. Solids* **1996**, *57*, 1851.

(26) van Elp, J.; Searle, B. G.; Sawatzky, G. A.; Sacchi, M. *Solid State Commun.* **1991**, *80*, 67.

(27) Fischer, D. W. *J. Appl. Phys.* **1965**, *36*, 2048.

(28) Kawai, J.; Nakajima, K.; Gohshi, Y. *Spectrochim. Acta.* **1993**, *48B*, 1281.

(29) Kawai, J.; Nakajima, K.; Maeda, K.; Gohshi, Y. *Adv. X-ray Anal.* **1992**, *35*, 1107.

(30) Fujiwara, F.; Scimeca, T.; Ratnapala, L.; Andermann, G. *Spectrosc. Lett.* **1997**, *30*, 575.

(31) Butorin, S. M.; Galakhov, V. R.; Kurmaev, E. Z.; Glazyrina, V. I. *Solid State Commun.* **1992**, *81*, 1003.

(32) Wood, P. R.; Urch, D. S. *J. Chem. Soc., Dalton Trans.* **1976**, 2472.

(33) Grush, M. M.; Muramatsu, Y.; Underwood, J. H.; Gullikson, E. M.; Ederer, D. L.; Perera, R. C. C.; Callcott, T. A. *J. Elect. Spectrosc.* **1998**, *92*, 225.

(34) Underwood, J. H.; Gullikson, E. M.; Koike, M.; Batson, P. J. *SPIE* **1997**, *3113*, 214.

(35) Jia, J. J.; Callcott, T. A.; Yurkas, J.; Ellis, A. W.; Himpsel, F. J.; Samant, M. G.; Stohr, J.; Ederer, D. L.; Carlisle, J. A.; Hudson, E. A.; Terminello, L. J.; Shuh, D. K.; Perera, R. C. C. *Rev. Sci. Instrum.* **1995**, *66*, 1394.

measurements (Mn, $\geq$670 eV; Co, $\geq$825 eV; Ni, $\geq$ 900 eV). The soft X-ray fluorescence endstation[35] consists of a Rowland circle-type emission spectrometer with a fixed entrance slit and a 1500 lines/mm grating mounted on a 10-m Rowland circle. The X-ray fluorescence is refocused onto a multichannel plate area detector, enabling the entire emission spectrum to be obtained without scanning the detector. With an entrance slit of 50 μm, the resolution of this detector corresponds to ~1.1 eV in the Mn fluorescence region and 1.6 and 2.0 eV in the Co and Ni fluorescence regions, respectively. Mn emission spectra were calibrated relative to the L$_\beta$ emission of MnO;[36] Co and Ni emission spectra were calibrated relative to the L$_{\alpha,\beta}$ emission of Co and Ni foils, respectively.[37] All emission spectra were set to zero intensity ~20 eV above the L$_{\alpha,\beta}$ emission, normalized to unit intensity at the L$_\beta$ peak, and smoothed over a 13-point region using the commercially available program *Origin*.

The LiMn$_2$O$_4$ and LiMn$_{2-y}$Me$_y$O$_4$ ($y \leq 0.25$ and Me = Co, Ni, Li) samples were prepared by grinding together stoichiometric amounts of MnO$_2$ (CMD, Japan Metals and Chemicals), LiOH$\cdot$H$_2$O (Spectrum Chemical), and NiCO$_3$ (Alfa-Aesar) or CoCO$_3$ (JT Baker) in *n*-hexane. The mixtures were twice heated in air at 20 °C/min to 750 °C for 40 h on a preconditioned alumina boat, cooled at 0.8 °C/min, and reground in *n*-hexane. Highly substituted spinels ($y > 0.25$) were synthesized using all carbonate precursors (Li$_2$CO$_3$ and MnCO$_3$ from JT Baker). The synthesis conditions were identical to those mentioned above except for dwell times of 36 h for LiMn$_{1.5}$-Co$_{0.5}$O$_4$ and 120h for LiMn$_{1.5}$Ni$_{0.5}$O$_4$. Further details concerning the synthesis of the Mn-substituted compounds can be found elsewhere.[38] NiO and CoO were used as obtained from Aldrich Chemical Co.; LiCoO$_2$ and LiNiO$_2$ were used as obtained from Merck/EM Science.

The structures of all LiMn$_2$O$_4$ and LiMn$_{2-y}$Me$_y$O$_4$ samples were confirmed by X-ray powder diffraction measurements. The LiMn$_{1.75}$Ni$_{0.25}$O$_4$ and LiMn$_{1.5}$Ni$_{0.5}$O$_4$ may have contained a small amount (<2 wt %) of a Li$_{1-x}$Ni$_x$O impurity phase as discussed elsewhere.[39] However, the lattice parameters of these compounds agreed with those published for pure LiMn$_{1.75}$-Ni$_{0.25}$O$_4$ and LiMn$_{1.5}$Ni$_{0.5}$O$_4$ samples.[39] For the series of LiMn$_{2-y}$Me$_y$O$_4$ electrode materials (Me = Co, Ni, Li) used in this study, a linear correlation between the relative percentage of Mn^{3+} and the initial capacity was obtained ($r^2 = 0.988$).

Samples run in the fluorescence endstation were finely powdered, either pressed into pellets or layered on Si wafers, and mounted in the chamber at a grazing angle of ~22° with respect to the incoming beam. Pellets for Mn absorption experiments were affixed to a sample slide that was placed perpendicular to the incoming X-ray beam.

Results and Discussion

The Co and Ni L-absorption data from a series of LiMn$_{2-y}$Me$_y$O$_4$ electrode materials (Me = Co, Ni) and model compounds are shown in Figure 1. There are two main peaks in the spectra which are due to electronic transitions to the 3d levels from the 2p$^{3/2}$ and 2p$^{1/2}$ levels and are denoted L$_{III}$ and L$_{II}$, respectively.

For the electrode materials, the Co L$_{III}$ peak occurs at 780.5 eV and the L$_{II}$ is at 794.8 eV (Figure 1, left). Within the signal-to-noise of the data, the LiCo$_y$Mn$_{2-y}$O$_4$ spectra are virtually unchanged with increasing amounts of cobalt substitution. The sharp peaks with high-energy shoulders in both the L$_{III}$ and L$_{II}$ regions and a low
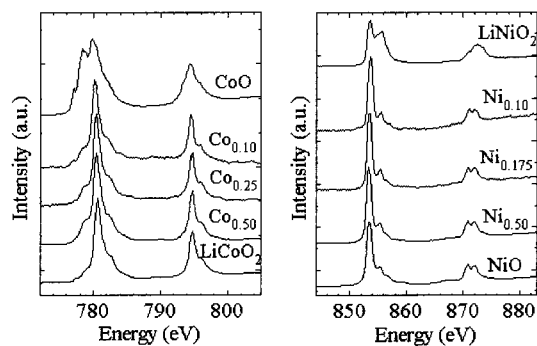
Figure 1. Co and Ni L-absorption spectra of LiMn$_{2-y}$Me$_y$O$_4$ electrode materials (Me = Co, Ni): (left) Co L-absorption spectra from Co(II)O, three samples with different amounts of Co substitution ($y = 0.10, 0.25, 0.50$), and LiCo(III)O$_2$ and (right) Ni L-absorption spectra from LiNi(III)O$_2$, three samples with different amounts of Ni substitution ($y = 0.10, 0.175, 0.50$), and Ni(II)O.

energy shoulder in the L$_{III}$ region strongly resemble the experimental spectrum of LiCo(III)O$_2$. Co(II) spectra, as demonstrated by the spectrum of Co(II)O, have multiple features in the L$_{III}$ region which cover a larger energy range and also exhibit a broader L$_{II}$ peak than Co(III) spectra. This contrast in Co(II) versus Co(III) spectral features has been observed previously and can be simulated with atomic multiplet calculations.[23,24] We therefore conclude that the cobalt substitutes for manganese in LiMn$_{2-y}$Me$_y$O$_4$ electrode materials as Co(III) and remains unchanged upon higher levels of cobalt substitution. Our results confirm an earlier electron energy loss study by Suzuki et al.[25] that suggested an oxidation state of Co(III) in LiMnCoO$_4$. To our knowledge, spectroscopic determination of the cobalt oxidation state in LiMn$_{2-y}$Co$_y$O$_4$ ($0 \leq y < 0.5$) electrode materials has not been previously demonstrated in the literature.

The two main peaks in the L$_{III}$ and L$_{II}$ regions of the Ni L-absorption spectra occur at 853.4 and 871.0 eV, respectively (Figure 1 right), for the electrode materials. The spectra are again virtually unchanged with increasing amounts of substitution, within the signal-to-noise of the data. The sharp L$_{III}$ peak with a resolved high-energy shoulder and the L$_{II}$ region split into two partially resolved peaks with intensity only slightly higher for the low-energy feature are practically identical to the features observed for the experimental spectrum of Ni(II)O and very different from the broader features expected in both the L$_{III}$ and L$_{II}$ regions of Ni-(III) spectra, represented here by the spectrum of LiNi-(III)O$_2$. This dependence of the shape of Ni spectra on oxidation state has been demonstrated earlier and simulated with atomic multiplet calculations.[26] The Ni L-edges confirm the results of a photoemission study,[11] which suggested that the nickel is present as Ni(II) in LiMn$_{1.5}$Ni$_{0.5}$O$_4$. Our results also indicate that the nickel oxidation state is independent of the degree of metal substitution. In addition, we mention that the L-edge technique is a precise way to probe oxidation state changes that is also applicable to in situ measurements of LiMn$_{2-y}$Me$_y$O$_4$ electrode materials.

By using the oxidation state values of +1 for Li, +2 for Ni, and +3 for Co, the nominal Mn oxidation state can be calculated for the LiMn$_{2-y}$Me$_y$O$_4$ electrode materials (Me = Li, Co, Ni and $0 \leq y \leq 0.5$) used in this study. Mn L-absorption data from two series of these

(36) Butorin, S. M.; Guo, J.-H.; Magnuson, M.; Kuiper, P.; Nordgren, J. *Phys. Rev. B* **1996**, *54*, 4405.

(37) Henke, B. L.; Lee, P.; Tanaka, T. J.; Shimabukuro, R. L.; Fujikawa, B. K. *At. Data Nucl. Data Tables* **1982**, *27*, 46.

(38) Horne, C. R. Ph.D. dissertation, University of California, Berkeley, 1999.

(39) Zhong, Q.; Bonakdarpour, A.; Zhang, M.; Gao, Y.; Dahn, J. R. *J. Electrochem. Soc.* **1997**, *144*, 205.
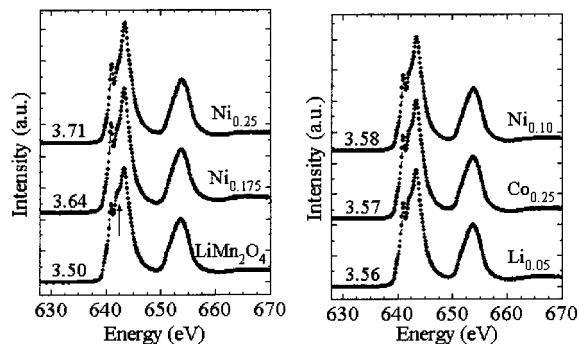
Figure 2. Mn L-absorption spectra of $LiMn_{2-y}Me_yO_4$ electrode materials (Me = Co, Ni, Li): (left) three different amounts of Ni-substitution resulting in nominal oxidation states for Mn of 3.50 ($y = 0.00$), 3.64 ($y = 0.175$), 3.71 ($y = 0.25$) and (right) three different types of metal substitution (Me = Co, Ni, Li) resulting in approximately the same Mn oxidation state.

Figure 3. Mn L-emission spectra of $LiMn_{2-y}Ni_yO_4$ electrode materials: (left) three different amounts of Ni-substitution ($y = 0.00, 0.175, 0.25$) and (right) a typical simulation (solid line) of the data (circles) and the component Lorentzians (dotted lines) of the simulation.

samples are presented in Figure 2. The nominal Mn oxidation state is shown to the left of each spectrum, increasing from 3.50 to 3.71 for different amounts of Ni substitution (Figure 2, left). The two main peaks in the spectra, L_{III} and L_{II}, occur at approximately 643.4 and 653.8 eV, respectively. There are several resolved features observable in the L_{III} region which are presumably the result of multiplet splittings. Although atomic multiplet calculations have been successfully applied to Mn(II) compounds,[22,24] charge transfer (covalency) and lower symmetry become more important for Mn(III) and Mn(IV) and theoretical simulations have to date not been successful.

The main difference between the three nickel-substituted spectra presented here is the shoulder marked with an arrow which arises from the convolution of 50% Mn(III) and 50% Mn(IV) in $LiMn_2O_4$ and decreases as the system comes closer to containing pure Mn(IV). In addition, the main L_{III} peak shifts to slightly higher energy upon increasing the oxidation state of the Mn. The energy shifts are roughly 0.1 eV for each increase in nominal manganese oxidation state of ~0.1. The magnitude of this shift is small, as expected—for oxidation from pure Mn(III) to Mn(IV), an edge shift on the order of 1 eV is typically obtained. We note that an earlier study[16] misinterpreted Mn XAS data of $LiMn_2O_4$, concluding from Mn L- and K-edge data that all of the manganese was present as Mn(IV). This has been shown to be an incorrect interpretation from K-edge simulations[17] and Mn K_β emission results.[5] In addition, it does not agree with other published Mn(IV) and mixed-valent Mn(III)Mn(IV) L-edge spectra.[21,22]

The right panel of Figure 2 shows three spectra from substituted electrode materials with approximately the same nominal oxidation state, 3.57 ± 0.01, but with varying amounts of Co, Ni, or Li substitution. The energy of the main L_{III} peak remains constant for the three spectra. In addition, there are no significant changes in the shape of the spectra. This indicates that the manganese in all three systems have the same oxidation and spin states and that no major geometric rearrangement occurs dependent on the type of metal substituent.

Figure 3 presents the manganese L-edge XES spectra from the same series of Ni-substituted $LiMn_2O_4$ electrodes as shown in the left panel of Figure 2. The $2p^{3/2}$
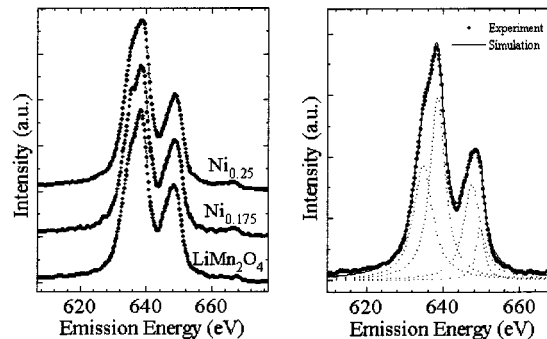
and $2p^{1/2}$ core holes created by the absorption process can be filled by 3d electrons, giving rise to the L_α (637.5 eV) and L_β (648.5 eV) emission, respectively. Upon increasing the nominal Mn oxidation state by a higher level of Ni substitution, the intensity of the L_α peak (with respect to the intensity of the L_β peak) increases, indicating a greater degree of covalency. Although Mn(II) resonant XES spectra have been simulated by atomic multiplet calculations,[36] this method has not been successfully applied to higher valent Mn compounds. Moreover, quantitative simulation of transition metal XES excited above threshold has remained elusive, at least partially due to the initial state having a core hole that is not well defined. However, a qualitative understanding of the spectra is possible and can be informative, as discussed in the following paragraphs.

The Mn valence band contains contributions from both the transition metal and the ligands. States with predominantly O 2p character but containing some Mn 3d character can also contribute to the $L_{\alpha,\beta}$ emission. These states will be more tightly bound and therefore the emission will be observed at lower energy than emission from states with predominantly Mn 3d character. An increase in covalency will result in a larger occupancy of the mixed O 2p–Mn 3d part of the band and thus an increase in the intensity of the lower energy side of the L_α region will be observed (see Figure 3, left panel). This effect has been previously discussed in relation to Mn L-XES.[32,40] A similar rationale has been used together with configuration interaction theory[41] and with electronic density of states LMTO calculations[40] to simulate the XPS of MnO.

We note that the L_α/L_β ratio of Cu compounds has been shown to be affected by changes in concentration (self-absorption).[29] Due to the proximity of the Cu L_β emission to the Cu L_{III} absorption threshold, self-absorption of the L_β emission can occur. In this process, a $2p^{1/2}$ core hole is filled and the resulting L_β photon creates a $2p^{3/2}$ core hole that can then be filled by a 3d electron, leading to L_α fluorescence. The L_β photon can also be absorbed by other Cu atoms and thus an increase in the concentration of Cu in alloys enhances

(40) Galakhov, V. R.; Butorin, S. M.; Kurmaev, E. Z.; Korotin, M. A. *Physica B* **1991**, *168*, 163.
(41) Fujimori, A.; Kimizuka, N.; Akahane, T.; Chiba, T.; Kimura, S.; Minami, F.; Siratori, K.; Taniguchi, M.; Ogawa, S.; Suga, S. *Phys. Rev. B* **1990**, *42*, 7580.

this effect. However, we did not see any evidence for concentration dependence of the L_α/L_β ratio in the Mn powders we have previously examined.[33] Additionally, increasing the Ni substitution would result in a decrease in the Mn concentration and thus a decrease in self-absorption would be expected (smaller L_α/L_β ratio). However, the dominant effect (see Figure 3) upon increased Ni substitution is an increase in the L_α/L_β ratio.

In addition, Cu compounds have been shown to have L_α/L_β ratios which decrease with an increase in oxidation state[29]—in contrast to the increase in L_α/L_β ratio we see with Mn(II) through Mn(IV) compounds. As Cu is oxidized, this change is accompanied by an increase in the band gap from Cu metal (0 eV band gap) to Cu(I) (semiconductors) to Cu(II) (semiconductors or insulators). Increasing the band gap will decrease the rate of $L_2 - L_3V$ Coster–Kronig decay. A $2p^{3/2}$ core hole is again generated at the expense of a $2p^{1/2}$ core hole but, in this case, a valence band electron is promoted to the conduction band. The smaller the band gap, the more likely the possibility of Coster–Kronig decay, the larger the number of $2p^{3/2}$ core holes and chance of L_α fluorescence, and thus the inverse correlation of the L_α/L_β ratio with oxidation state in Cu compounds.[29] This also explains why Mn metal has a much larger L_α/L_β ratio than oxidized Mn compounds which are typically classified as insulators. We therefore do not expect $L_2 - L_3V$ Coster–Kronig decay to play a significant role in the dependence of the L_α/L_β ratio on the oxidation state of the Mn compounds measured in this study.

The correlation of the increase in L_α/L_β ratio with increase in covalency is thought to play the predominant role in the oxidation state dependence of the L_α/L_β ratio for Mn(II) through Mn(IV) compounds.[32] To quantify this correlation of increased covalency with higher Mn oxidation states, the Mn L-XES spectra from a series of $LiMn_{2-y}Me_yO_4$ electrode materials (Me = Co, Ni, Li) with nominal Mn oxidation states within the range of 3.5–3.7 were simulated with a series of Lorentzians. The L_α/L_β ratio is then obtained by adding the integrated areas of the Lorentzian components of the L_α peak and dividing this quantity by the sum of the integrated areas of the L_β Lorentzian components. The minimum number of Lorentzians needed was found to be four and a typical simulation is shown in the right panel of Figure 3. Because of experimental broadening, the L_β region can include a contribution from the elastic scatter, even with excitation well above the absorption threshold. In the case of slightly different excitation energies, varying amounts of the low-energy "tails" of the elastic peak contribute to the L_β region. To compensate for this effect, the L_α/L_β ratios were divided by the L_α/L_β of a sample of $LiMn_2O_4$ that was recorded under the same experimental conditions. We will hereafter refer to this quantity as the relative covalence. To confirm the validity of this arbitrary normalization procedure, the L_α/L_β ratios from two different electrode materials were plotted versus several above-threshold excitation energies (data not shown). Both sets of data were found to have the same slope.

The dependence of the relative covalence on partial metal substitution of $LiMn_2O_4$ by Co, Ni, and Li is shown in Figure 4 and Table 1. As the manganese oxidation state is increased by increased substitution with Co, the covalency of the Mn is increased. A similar
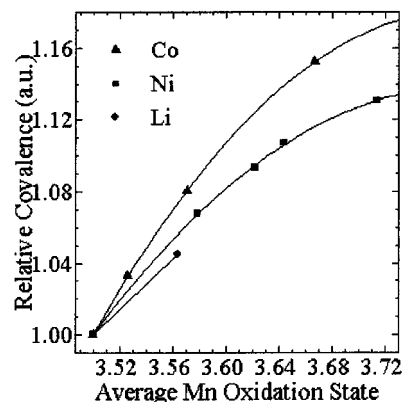
Figure 4. Dependence of the relative covalence of $LiMn_{2-y}Me_yO_4$ electrode materials on the nominal Mn oxidation state. Me = Li (circle), Co (triangles), Ni (squares).

Table 1. Parameters of LiMn₂O₄-Based Electrode Materials

sample $LiMn_{2-y}Me_yO_4$	av Mn oxidation state	L_α/L_β ratio
$y = 0$	3.500	1.000
Me = Co, $y = 0.10$	3.526	1.033
Me = Co, $y = 0.25$	3.571	1.081
Me = Co, $y = 0.50$	3.667	1.152
Me = Ni, $y = 0.10$	3.579	1.068
Me = Ni, $y = 0.15$	3.622	1.093
Me = Ni, $y = 0.175$	3.644	1.107
Me = Ni, $y = 0.25$	3.714	1.131
Me = Li, $y = 1.05$	3.564	1.045

trend is observed for Ni substitution. In addition, for a given average nominal Mn oxidation state, a sample substituted with Co is more covalent than one substituted with Ni which is in turn more covalent than a sample with Li substitution. (Again, the observed trend is the opposite of what would be expected if the concentration of Mn in these spinels was playing a dominant role in the L_α/L_β ratio.) We have correlated the calculated percent covalency for MnO_6 octahedra[42] with our previously published Mn L-emission data[33] for different oxidation states of Mn. We estimate that a 1% increase in the Mn L_α/L_β ratio corresponds to an increase in covalency of ~1.6%. Thus, at a nominal manganese oxidation state of 3.56, the Co-substituted sample is ~3% more covalent than the Ni-substituted sample which is in turn ~2% more covalent than the Li-substituted sample. Increasing the nominal Mn oxidation state increases the divergence of the relative covalence curves. At a nominal Mn oxidation state of 3.64, the difference in the Mn covalency between Co- and Ni-substituted samples becomes ~5%.

Figure 5 shows the Co and Ni L-emission spectra of several of the substituted $LiMn_{2-y}Me_yO_4$ electrode materials ($y = 0.10, 0.50$). The main peaks of the Co $L_{\alpha,\beta}$ emission occur at approximately 777.3 and 791.7 eV and the Ni $L_{\alpha,\beta}$ at 851.8 and 868.9 eV. Both the Co and the Ni emission spectra show little change with increased levels of substitution. Only a very slight narrowing of the L_α peak is observed when the substitution level is raised to $y = 0.50$ from $y = 0.10$. (Contrast with Figure 3 where y varies from 0 to 0.25 in Ni-substituted $LiMn_{2-y}Me_yO_4$ electrode materials.) This suggests that the electronic structure of the Ni or Co substituent is relatively unaffected by increased sub-

(42) Sherman, D. M. *Am. Mineralog.* **1984**, *69*, 788.
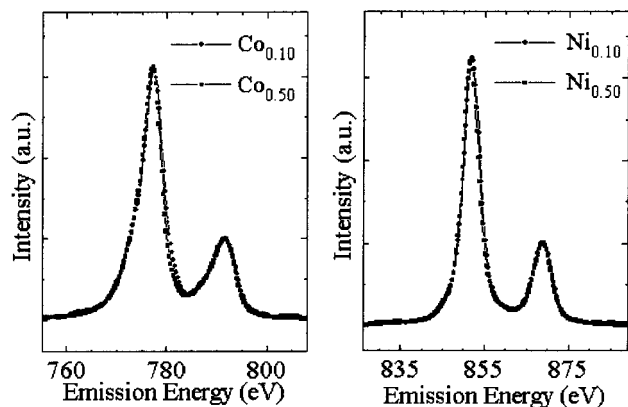
Figure 5. Co and Ni L-emission spectra of LiMn$_{2-y}$Me$_y$O$_4$ electrode materials (Me = Co, Ni): (left) Co L-emission spectra from two samples with different amounts of Co-substitution (y = 0.10, 0.50) and (right) Ni L-emission spectra from two samples with different amounts of Ni-substitution (y = 0.10, 0.50).

stitution, at least up to the levels of substitution presented here.

Conclusions

By using Co and Ni L$_{II,III}$-edge XAS as a fingerprint technique, we have shown that cobalt substitutes for manganese as Co(III) and nickel as Ni(II) in LiMn$_{2-y}$Me$_y$O$_4$ electrode materials ($y \leq 0.5$). The oxidation state of the metal substituent is invariant with respect to the level of substitution in the LiMn$_{2-y}$Me$_y$O$_4$ electrode materials ($y \leq 0.5$) studied here.

The Mn L-absorption spectra of LiMn$_{2-y}$Me$_y$O$_4$ electrode materials (Me = Co, Ni, Li) reflect the nominal average Mn oxidation state of the LiMn$_2$O$_4$-based electrode materials. In addition, the electronic structure surrounding the substituent (Co or Ni), as probed by both XAS and XES at the Co and Ni L-edges is relatively unaffected by increased levels of substitution. These results clearly do not explain the differences in substituent-dependent cycling behavior as seen by researchers such as W. Liu et al.[10]

In contrast, by using the technique of Mn L-emission to probe the covalency of LiMn$_{2-y}$Me$_y$O$_4$ electrode materials (Me = Co, Ni, Li), we have shown that for a given nominal Mn oxidation state, the manganese covalency of Co-substituted electrode materials is greater than that with Me = Ni which is greater than that for Me = Li. This increase in covalency of LiMn$_{2-y}$Me$_y$O$_4$ electrode materials with Me = Co as compared to Me = Ni mirrors the increase in capacity retention as seen by W. Liu et al.[10] Greater covalency is expected to be beneficial to electrode performance. The more covalent the Mn−O bond, the stronger the bond, making the spinel structure more resistant to the destructive expansion and contraction observed in LiMn$_2$O$_4$ electrodes.

As the capacity retention and manganese covalency increase, the crystal radius of the substituent is decreasing (effective crystal radius: Li$^+_{oct}$ = 0.90 Å,
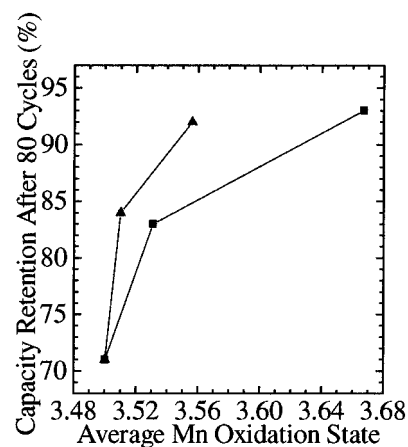
Figure 6.

Ni$^{2+}_{oct}$ = 0.83 Å, Co$^{3+}_{oct}$ = 0.69 Å[43]) while the oxidation state of the substituent is increasing (Li$^+$ < Ni^{2+} < Co^{3+}). Further experiments with different types of metal substitutions will help to determine the driving force for the observed differences in manganese covalency to allow further feedback for battery development.

We have shown that integrated intensity ratios of Mn L$_\alpha$ and L$_\beta$ emission can be used to determine the relative covalency of potential electrode active materials. The positive correlation observed between manganese covalency and capacity retention provides an explanation of improved cycling properties as a function of metal substitution. This knowledge provides important feedback for the engineering of higher performing rechargeable battery materials.

Appendix

Capacity Retention of LiMn$_2$O$_4$-Based Electrode Materials (data taken from Liu and co-workers[10]), shown both in figure (Figure 6, Co (triangles), Ni (squares)) and table (Table 2) format.

Table 2

sample LiMn$_{2-y}$Me$_y$O$_4$	av Mn oxidation state	capacity retention after 80 cycles (%)
y = 0	3.50	71.2
Me = Ni, y = 0.04	3.53	83.0
Me = Ni, y = 0.20	3.67	93.1
Me = Co, y = 0.04	3.51	84.3
Me = Co, y = 0.20	3.56	92.4

CM990366E

(43) Shannon, R. D. *Acta Crystallogr.* **1976**, *32*, 751.